Vibronic Activity in the Phosphorescence Spectra of Disklike Aromatic Molecules: A Combined Experimental and Theoretical Investigation

D. Baunsgaard[†] and N. Harrit*

Department of Chemistry, University of Copenhagen, Symbion, Fruebjergvej 3, DK-2100 Copenhagen, Denmark

M. El Balsami, F. Negri,* and G. Orlandi

Dipartimento di Chimica "G. Ciamician", Università di Bologna, 40126 Bologna, Italy

J. Frederiksen and R. Wilbrandt*

Condensed Matter Physics and Chemistry Department, FYS-313, Risø National Laboratory, DK-4000 Roskilde, Denmark

Received: July 6, 1998; In Final Form: September 16, 1998

The phosphorescence spectra of triphenylene and truxene, recorded in glassy solvents at 77 K, are presented. Their vibronic structure is interpreted on the basis of intensities computed with the help of quantum-chemical calculations. It is shown to be due to Herzberg−Teller-active nontotally symmetric modes which provide false origins for progressions of totally symmetric modes. Similarly to benzene, the dominant contribution to the $T_1 \rightarrow S_0$ transition in the two disklike molecules is shown to derive from triplet−triplet transition dipole moments. Radiative triplet lifetimes are estimated on the basis of computed oscillator strengths and compared with the correspondingly observed values.

1. Introduction

Triphenylene (TPH) and truxene (TN) are two examples of highly symmetric polycyclic aromatic hydrocarbons. Some of their derivatives show self-organizing properties and form discotic liquid-crystalline phases. The supramolecular organization has attracted considerable attention in the field of material science since excitation or charge-transport phenomena are expected to be quasi one-dimensional for these systems, which therefore have been suggested as potential *molecular energy guides*.[1] A detailed knowledge of the electronic structure and properties of the isolated chromophores is the preliminary requirement to elucidate the mechanism of electronic transport in columnar phases. At the same time, the high symmetry and medium molecular size make these systems attractive to explore the effects of increasing molecular complexity by comparing their photophysical properties with those of the prototypical aromatic molecule, benzene.

In this study, we focus on the photophysics of the lowest triplet state and present a combined experimental and theoretical study of the phosphorescence of TPH and TN. TPH has been the subject of several studies, and its triplet manifold was investigated experimentally and theoretically.[2−5] In particular, the high-resolution phosphorescence spectrum, obtained in *n*-octane at 4.2 K by Nishi and co-workers,[2] shows a number of bands in the region of fundamentals, where nontotally symmetric (NTS) modes are active. Conversely, little information is provided on the activity of totally symmetric (TS) vibrations. Surprisingly, TN has received comparably less attention than TPH: a report on the position of the main bands in the phosphorescence spectrum appeared several years ago,[6] and since then no additional experimental data have been published. Very recently, triphenylene and its alkylsulfanyl-, alkylsulfonyl-, and alkyloxy-substituted derivatives were investigated[7] and the effect of substituents on the photophysical properties was examined. Here, we reconsider the phosphorescence spectrum of TPH and present the phosphorescence spectrum of TN. The spectra, recorded in glassy solvents (methylcyclohexane and ethanol) at 77 K, show peculiar vibronic structures in the region of fundamentals and combination bands. These were analyzed on the basis of quantum-chemical calculations followed by simulation of the spectra in order to extract information on active vibrational motions. Similarly to benzene, the phosphorescence of TPH and TN are both symmetry and spin forbidden. Hence, the simulation of vibronic intensities required the inclusion of spin−orbit along with vibronic perturbations that were calculated with the semiempirical approach recently employed to analyze the phosphorescence spectrum of the fullerene C_{70}.[8]

2. Experimental Section

The phosphorescence spectrum of triphenylene was recorded at 77 K on a LS 50B Perkin-Elmer luminescence spectrometer using the phosphorescence accessory. Triphenylene was dissolved in methylcyclohexane (MCH) to a concentration of 10^{-7} M and measured in a 2 mm quartz tube submerged in liquid nitrogen. The spectral resolution was 5.0 nm. The phosphorescence spectrum of truxene was measured at 77 K in ethanol in a cryostat (Oxford Instruments DN1704) by excitation with light from a pulsed Excimer laser (Lambda Physik EMG102E) at 308 nm. The spectrum was detected by an optical multi-

[†] Present address: Department of Dairy and Food Science, The Royal Veterinary and Agricultural University, Rolighedsvej 30, DK-1958 Frederiksberg C, Denmark.

* Corresponding authors.

10.1021/jp982876m CCC: $15.00
Published on Web 11/14/1998

channel detector (OSMA IRY-700). The spectral resolution was 4 nm. The spectra were not corrected for variations of the detection sensitivity of the spectrometers with wavelength.

3. Computational Details

To analyze the vibronic structure of the phosphorescence spectra of TPH and TN, we carried out quantum-chemical calculations of equilibrium structures and vibrational force fields with the help of a modified version[9] of the QCFF/PI (quantum-consistent force field for π electrons) semiempirical method.[10] Electronic excitation energies and transition dipole moments were computed with the CNDO/S (complete neglect of differential overlap for spectroscopy) Hamiltonian,[11] combined with configuration interaction singles (CIS) calculations which included all the single excitations arising from the full valence orbital space for triphenylene (42 × 42, 1764 singly excited configurations (SECs)) and a comparably large orbital space (42 × 41, 1722 SECs) for truxene. The Pariser formula was employed to evaluate electron repulsion integrals. The calculation of the $S_0 \leftrightarrow T_1$ transition dipole moment requires the inclusion of the spin−orbit (SO) perturbation. The spin−orbit couplings $H_{S_K,T_j\infty}^{SO}$ between every singlet state S_k and the three components $\alpha = x, y, z$ of every triplet state T_j resulting from the CIS calculations described above were evaluated in the one-electron approximation, according to the approach of ref 12

$$H_{S_k,T_j\alpha}^{so} = \langle S_k | \sum_n \sum_A \zeta_A \mathbf{l}_n \cdot \mathbf{s}_n | T_j^{\alpha} \rangle \tag{1}$$

where $\mathbf{l}_n$ and $\mathbf{s}_n$ are orbital and spin angular momentum operators of the nth electron, A runs over the atoms of the molecule, and ζ_A is the SO constant for atom A.[12] The spin−orbit-induced transition dipole moment was computed according to first-order perturbation theory

$$M_{S_0,T_1} = \sum_k M_{S_0,S_k} \frac{H_{S_k,T_1}^{so}}{(E_1 - E_k)} + \sum_m \frac{H_{S_0,T_m}^{so}}{(E_0 - E_m)} M_{T_m,T_1} \tag{2}$$

In the expression above, k and m run over the full space of singlet and triplet states considered in the CIS calculations. Similarly to benzene, the above transition dipole moment is zero by symmetry for TPH and TN. This implies that the vibronic structure of the phosphorescence spectra is dominated by Herzberg−Teller (HT) induced false origins. Thus, the estimate of the $0 \rightarrow 1$ vibronically induced intensity in the phosphorescence spectrum (0 and 1 being the initial and final vibrational quantum numbers of the lth NTS mode) required additional evaluation of the numerical derivatives of the M_{S_0,T_1} transition dipole moment with respect to each normal coordinate Q_l which may be active on the basis of symmetry selection rules:

$$M_{S_0,1_l \leftarrow T_1,0_l} = \left[\frac{\partial}{\partial Q_1} M_{S_0,T_1}(Q) \right]_0 \int \lambda_1^{S_0} Q_l \lambda_0^{T_1} \, \mathrm{d}Q_l \tag{3}$$

The vibronic transition moment in eq 3 is readily obtained by integration over the vibrational integral, which in the harmonic approximation is equal to $(\hbar/2\omega_l)^{1/2}$. Conversely, the Franck−Condon (FC) activity of the ith TS mode in the spectra is governed by the displacement parameter B_i defined as

$$B_i = \left(\frac{\omega_i}{\hbar} \right)^{1/2} Q_{i(S_0)}^{T_1,S_0} \tag{4}$$

Here $Q_{i(S_0)}^{T_1,S_0}$ is the projection of the geometry change between the two states S_0 and T_1, expressed in Cartesian coordinates, onto the S_0 state normal coordinate $Q_i^{S_0}$, that is

$$\mathrm{Q}_{i(S_0)}^{T_1,S_0} = [\mathbf{x}_{T_1} - \mathbf{x}_{S_0}] \mathbf{M}^{1/2} \mathbf{L}_i^{S_0} \tag{5}$$

where $\boldsymbol{x}_K$ is the $3N$-dimensional vector of the equilibrium Cartesian coordinates in the Kth state, $\boldsymbol{M}$ is the $3N \times 3N$ diagonal matrix of the atomic masses, and $\boldsymbol{L}_i^{S_0}$ is the $3N$ vector describing the normal coordinate $Q_i^{S_0}$, in terms of mass-weighted Cartesian coordinates. Under the harmonic approximation, the ratio between the intensity of a member of the progression in the ith TS mode and the 0−0 band is given by

$$\frac{I_i(v)}{I(0-0)} = \frac{(\gamma_i)^v}{v!} \tag{6}$$

where v is the vibrational quantum number of the TS mode and $\gamma_i = {}^1/_2 B_i^2$. Since the phosphorescence of TPH and TN are both symmetry and spin forbidden, TS modes can only form progressions built on NTS fundamentals which gain intensity vibronically. Similarly, relation 6 also holds for the ratio between the intensity of the members of a progression built on a false origin and the intensity of the false origin. Radiative lifetimes τ°_r associated with the phosphorescence process were computed from the calculated vibronically induced oscillator strengths with the following expression[13]

$$\tau^\circ_r = \frac{1.4758}{\nu^2 n^2 f} \tag{7}$$

where ν is the $S_0 - T_1$ energy difference, n is the refractive index of the solvent, and f is the total oscillator strength. At 77 K, where full equilibration among the three triplet sublevels occurs, each sublevel contributes, on average, ${}^1/_3$ of the total population and, consequently, the oscillator strength in eq 7 is ${}^1/_3$ of the total computed oscillator strength.

4. Results

The molecular structure and atom numbering of TN and TPH are shown in Figure 1a and 1b, respectively. The phosphorescence spectra recorded at 77 K are presented in the top part (spectra A) of Figures 2 and 3 for TN and TPH, respectively, and the correspondingly observed peak positions are listed in the first and fourth columns of Table 1. Interestingly, besides the activity in the region of fundamentals, several bands are observed in the region of combination bands where progressions of TS vibrations built on false origins can contribute intensity.

The results of quantum-chemical geometry optimization, carried out with a modified version[9] of the QCFF/PI method, are summarized in Table 2. According to these calculations, the S_0 and T_1 equilibrium structures of TPH both belong to D_{3h} symmetry. Conversely, the C_{3h} structure of TN in T_1 is not a minimum on the potential-energy surface. Indeed, further energy minimization leads to a slightly distorted minimum belonging to C_s symmetry and stabilized by only 160 cm^{-1}. The instability of the lowest triplet state of benzene derivatives is not surprising, since a mechanism similar to the pseudo Jahn−Teller (PJT) interaction which couples T_1 with the lowest E_{1u} state of benzene[14] is also likely to be operative in related systems, between T_1 and low-lying states of E symmetry. However, with such a small stabilization, the PJT distortion computed for TN becomes dynamic when the zero-point energy is taken into account. In this sense, we can neglect the effect

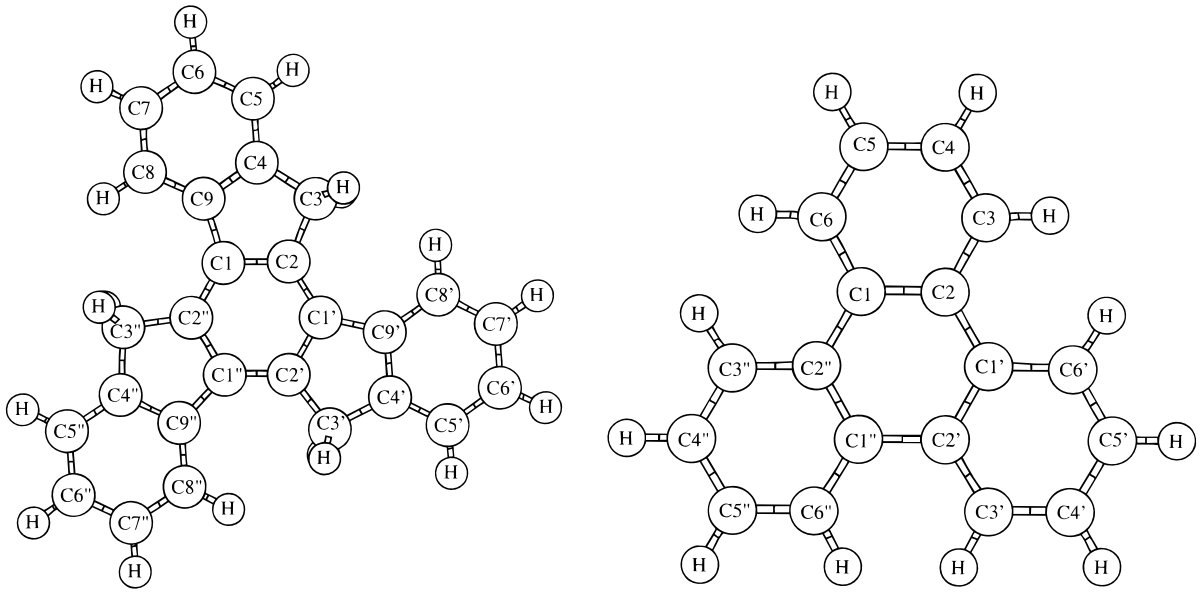

Figure 1. Carbon-atom numbering adopted for (a) truxene and (b) triphenylene.

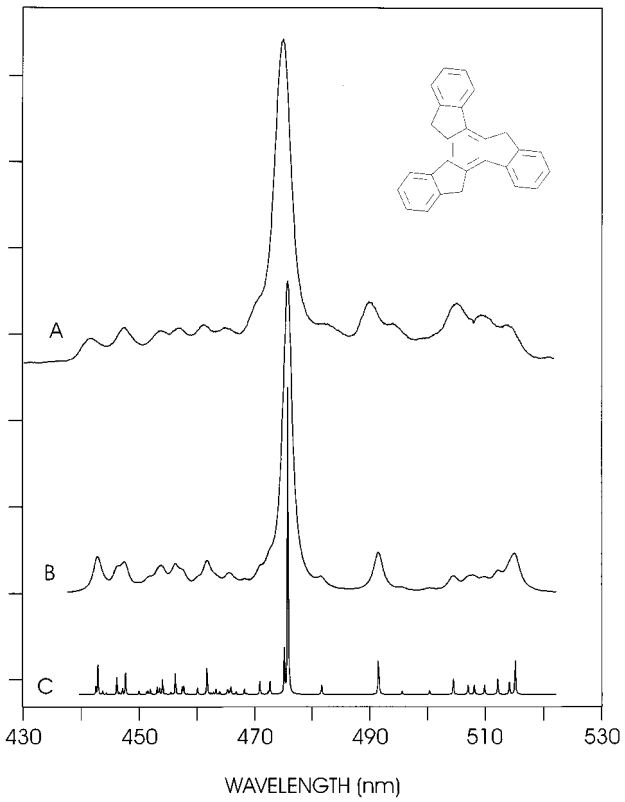

Figure 2. Phosphorescence spectrum of truxene: (A) spectrum observed in ethanol at 77 K; (B) low-resolution simulated spectrum (line width 40 cm^{-1}); (C) high-resolution simulated spectrum (line width 3 cm^{-1}). The 0−0 transition in the simulations was set to 22645 cm^{-1}.

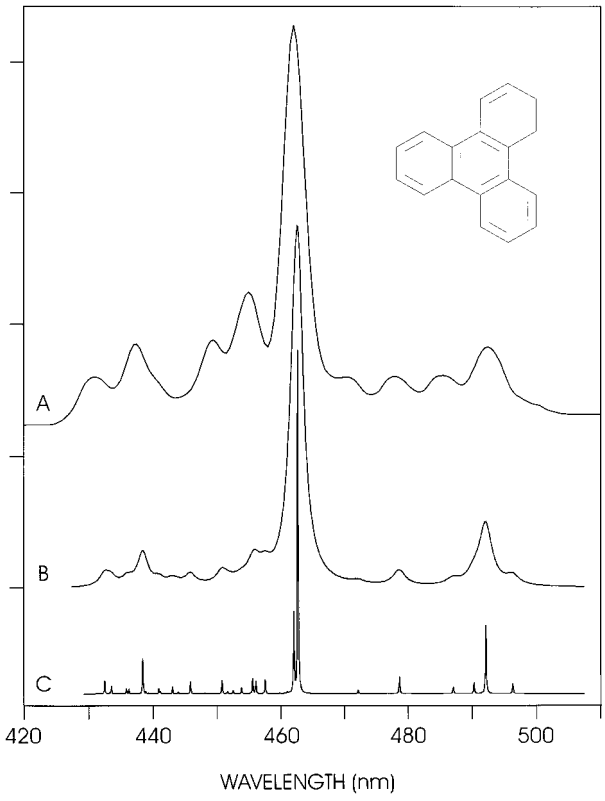

Figure 3. Phosphorescence spectrum of triphenylene: (A) spectrum observed in MCH at 77 K; (B) low-resolution simulated spectrum (line width 50 cm^{-1}); (C) high-resolution simulated spectrum (line width 3 cm^{-1}). The 0−0 transition in the simulations was set to 23202 cm^{-1}.

of symmetry lowering in the following discussion of the phosphorescence spectrum of TN, since the emitting state belongs, dynamically, to C_{3h} symmetry. Although QCFF/PI calculations might underestimate the PJT stabilization of the distorted structure of TN,[15] the simulations of the phosphorescence spectra of TPH and TN suggest that, similarly to benzene, the two systems are not permanently distorted in one conformation. Rather, the distortion, if existing, is dynamic and the molecule can make excursions over the entire potential-energy surface.

The lowest singlet and triplet states of TN and TPH resulting from CNDO/S + CIS calculations are presented in Table 3. Excitation energies are computed with satisfactory accuracy for both molecules, although $S_0 - T_1$ energy differences are slightly underestimated by the calculations. The triplet excitation energy of 20 485 cm^{-1} computed for TN can be compared with the 22 645 cm^{-1} value observed in ethanol, while the calculated 21 533 cm^{-1} value for $\Delta E(T_1 - S_0)$ of TPH can be compared with the 23 231 cm^{-1} value observed in *n*-octane[2] or with the 23 202 cm^{-1} excitation energy observed in MCH (see Table 1).

TABLE 1: Bands Observed in the Phosphorescence Spectra of Truxene and Triphenylene and Assignment Based on Simulated Vibronic Structures

truxene			triphenylene		
nm[a]	shift (cm^{-1})	assignment[b]	nm[c]	shift (cm^{-1})	assignment[b]
441.6	0−0	$0-0+47(a'')+65(e'')$	431.0	0−0	$0-0+79(e'')+134(a_1'')$
447.3	289	$230(a'')+305(e')$	437.4	340	$392(e')$
453.7	604	$575(e')+620(e')$	449.2	940	$1019(e')$
456.9	758	$727(a'')+796(e')$	454.9	1219	$1252(e')+1276(e')+1347\ (e')$
461.1	958	$988(e')$	462.1	1562	$1559(e')+1591(e')$
464.9	1135	$1150(e')+1156(e')+1181(e')$	470.7	1957(1562 + 395)	$1591(e')+431(a_1')$
470.4	1386	$1410(e')+1489(e')+1600(e')$	478.0	2281(1562 + 719)	$1591(e')+718(a_1')$
474.9	1588	$1629(e')$	485.4	2600(1562 + 1038)	$1591(e')+1079(a_1')$
482.5	1920(1588 + 332)	$1629(e')+254(a')$	492.5	2897(1562 + 1335)	$1591(e')+1216(a_1')+1292(a_1')$
490.0	2237(1588 + 649)	$1629(e')+670(a')+677(a')$			
494.2	2410(1588 + 822)	$1629(e')+839(a')$			
505.0	2843(1588 + 1255)	$1629(e')+1194(a')$			
509.4	3014(1588 + 1426)	$1629(e')+1294(a')+1336(a')+1404(a')$			
513.6	3175(1588 + 1587)	$1629(e')+1491(a')+1567(a')+1605(a')$			

[a] This work, bands observed in ethanol at 77 K. [b] Based on computed vibrational frequencies and intensities. [c] This work, bands observed in MCH at 77 K.

TABLE 2: Computed Bond Lengths (Å) and Angles (deg) of Truxene and Triphenylene in S_0 and T_1

bond	S_0[a]	T_1[a]	angle	S_0[a]	T_1[a]
			Truxene (C_{3h})		
C_1C_2	1.434	1.446	$C_1C_2C_3$	113.2	113.1
C_2C_3	1.509	1.507	$C_2C_3C_4$	99.6	99.4
C_3C_4	1.511	1.509	$C_3C_4C_9$	113.5	113.2
C_4C_5	1.397	1.390	$C_4C_5C_6$	118.4	118.5
C_5C_6	1.411	1.418	$C_5C_6C_7$	120.7	120.8
C_6C_7	1.409	1.417	$C_6C_7C_8$	120.9	121.1
C_7C_8	1.411	1.403	$C_7C_8C_9$	118.3	118.4
C_8C_9	1.401	1.416	$C_8C_9C_4$	120.7	120.3
C_9C_1	1.478	1.452	$C_9C_4C_5$	120.8	120.9
C_1C_2''	1.396	1.408	$C_1C_9C_4$	107.0	107.2
C_4C_9	1.424	1.440	$C_2C_1C_9$	106.8	107.0
			$C_2C_1C_2''$	120.1	119.9
			$C_1C_2C_1'$	119.9	120.1
			Triphenylene (D_{3h})		
C_1C_2	1.435	1.457	$C_1C_2C_3$	118.6	118.4
C_2C_3	1.426	1.433	$C_2C_3C_4$	121.4	121.5
C_3C_4	1.396	1.403	$C_3C_4C_5$	120.0	120.1
C_4C_5	1.406	1.410	$C_2''C_1C_6$	121.4	121.6
C_1C_2''	1.483	1.461			

[a] From QCFF/PI calculations.

Concerning the singlet manifold, we notice that the lowest two predicted excited states of TPH are inverted compared to the experimental observation.[16] However, the computed inversion will negligibly affect the prediction of the $T_1 \rightarrow S_0$ transition dipole moment. The latter, according to the perturbative expansion of eq 2, is determined by the sum of contributions due to SO interactions of S_0 with all triplet states and of T_1 with all singlet excited electronic states. Since T_1 and $S_{1,2}$ are $\pi\pi^*$ states, the corresponding SO interactions will be either zero by symmetry or very weak and contribute negligibly to M_{S_0,T_1}. The ground-state vibrational frequencies of the two aromatic molecules were computed with the above-mentioned modified version of the QCFF/PI program, which was shown to provide, on average, more accurate vibrational force fields for aromatic molecules.[9] The resulting wavenumbers are compared with available experimental values in Tables 4 and 5 for TN and TPH, respectively.

A survey of the data in Table 4 shows a satisfactory agreement between computed and infrared and Raman observed fundamentals[17] of TN. In Table 6, we compare the computed vibrational frequencies of TPH with fundamentals observed in Raman and infrared studies[3] and with those deduced from the analysis of the low-temperature phosphorescence spectrum.[2] Clearly, the aim of this work is not to provide an accurate ground-state vibrational force field for the two aromatic molecules but rather to account for the appearance of specific active vibrations in the phosphorescence spectra. Nevertheless, the quality of the computed force field is satisfactory enough to ensure that deviations from observed fundamentals should not exceed few tens of cm^{-1}. For this reason, we propose, for TPH, some reassignments which correspond to underlined frequencies in Table 5. First, we assign the band observed in ref 3 at 1320 cm^{-1} to the third highest a_2' fundamental of TPH (computed at 1346 cm^{-1}). Second, we suggest that the 1255 cm^{-1} fundamental, assigned in ref 3 to the above-mentioned a_2' fundamental, should be reassigned to the sixth highest e′ fundamental (computed at 1276 cm^{-1}). Concerning out-of-plane modes, the investigation of ref 3 provided assignments to a_2'' fundamentals but only an indication of either a_1'' or e″ symmetry for the remaining out-of-plane vibrations. In Table 5, we have attempted an assignment of both a_1'' and e″ fundamentals by choosing frequencies from the list provided in ref 3. In addition, we suggest that the 758 cm^{-1} unassigned observed band might correspond to one of the missing e″ fundamentals. As will be seen in the next section, the combination of computed vibrational frequencies and phosphorescence intensities supports most of the reassignments proposed here and suggests additional reassignments of TPH fundamentals.

5. Discussion

Before we start discussing the activity observed in the phosphorescence spectra of the two disklike molecules, it is of some interest to consider the results obtained with the method outlined in section 3 for a simpler aromatic molecule. Benzene is considerably smaller than TPH and TN, and the evaluation of vibronically induced transition moments according to eq 2, by summing over all singlet and triplet states resulting from full valence CIS calculations, requires a minimal computational effort. At the same time, because of the parentage with TPH and TN, test calculations carried out on benzene provide information on the performance of the method and on the accuracy we can expect for the larger aromatic molecules. Similarly to TPH and TN, the phosphorescence of benzene is symmetry and spin forbidden[18] and vibronically induced via e_{2g}, b_{2g}, and e_{1g} vibrational modes. e_{2g} modes dominate the observed intensity[18] by contributing 64% (ν_8, 1584 cm^{-1}), 24% (ν_9, 1174 cm^{-1}), 2% (ν_6, 608 cm^{-1}), and 0.2% (ν_7, 3030 cm^{-1}) of the total intensity, b_{2g} modes contribute 4.9% (ν_5, 1005 cm^{-1}) and

TABLE 3: Lowest Singlet and Triplet Electronic States of Truxene (CNDO/S + CIS 42 × 41 Calculations) and Triphenylene (CNDO/S + CIS 42 × 42 Calculations)

truxene

state	sym	E (eV)	f [a]	wave function composition[b]
S_0	A′	0.00		ground config.
S_1	A′	3.92	0.000	0.61(63−64), 0.61(62−65)
S_2	A′	3.93	0.000	0.59(62−64), 0.59(63−65)
S_3	E′	4.28	1.322	0.44(62−64), 0.44(63−65), 0.38(62−66)
S_4	E′	4.46	0.062	0.39(61−68), 0.36(62−67), 0.31(60−66)
S_5	A′	4.47	0.000	0.40(63−69), 0.39(62−68), 0.38(61−67)

state	sym	E (eV)	f [c]	wave function composition [b]
T_1	A′	2.54		0.58(62−65), 0.58(63−64)
T_2	E′	3.02	0.0000	0.38(63−66), 0.33(61−64), 0.28(62−64), 0.28(63−64), 0.28(62−65), 0.28(63−65)
T_3	A′	3.39	0.0000	0.36(59−69), 0.36(60−68), 0.34(63−70), 0.34(62−71)
T_4	E′	3.62	0.0026	0.46(62−65), 0.46(63−64)
T_5	A′	3.92	0.0000	0.56(63−65), 0.56(62−64)
T_6	E′	3.95	0.0018	0.43(61−68), 0.40(62−67), 0.29(63−68), 0.28(62−66)

triphenylene

state	sym	E (eV)	f [a]	wave function composition[d]
S_0	A'_1	0.00		ground config.
S_1	A'_2	3.67	0.0000	0.64(41−44), 0.64(42−43), 0.27(40−45)
S_2	A'_1	3.91	0.0000	0.65(41−43), 0.65(42−44), 0.24(40−48), 0.21(37−45)
S_3	E′	4.48	0.6375	0.61(41−45), 0.33(42−44), 0.33(41−43)
S_4	E′	4.55	0.1041	0.58(40−44), 0.37(41−46), 0.37(42−47)
S_5	E′	5.18	3.0961	0.55(41−44), 0.55(42−43), 0.28(40−46)

state	sym	E (eV)	f [c]	wave function composition[d]
T_1	A'_2	2.67		0.58(41−44), 0.58(42−43)
T_2	E′	3.24	0.0002	0.44(41−45), 0.39(40−44), 0.32(41−43), 0.32(42−44)
T_3	E′	3.65	0.0001	0.56(41−44), 0.56(42−43), 0.34(40−46), 0.31(39−45)
T_4	A'_1	3.91	0.0000	0.65(41−43), 0.65(42−44)
T_5	A'_2	4.06	0.0000	0.53(40−45), 0.42(41−47), 0.42(42−46), 0.34(38−44), 0.34(39−43)
T_6	E′	4.10	0.0005	0.46(41−48), 0.46(42−45), 0.38(37−44), 0.35(40−43)

[a] Computed $S_0 \rightarrow S_n$ oscillator strength. [b] The two numbers enclosed in parenthesis indicate the molecular orbitals involved in the single excitation; the symmetries of computed molecular orbitals ranging from $n = 59$ to $n = 71$ are E″, E″, A″, E″, E″ (occupied orbitals) and E″, E″, A″, A″, E″, E″, E″, E″ and (empty orbitals). [c] Computed $T_1 \rightarrow T_n$ oscillator strength. [d] The two numbers enclosed in parenthesis indicate the molecular orbitals involved in the single excitation; the symmetries of computed molecular orbitals ranging from $n = 37$ to $n = 48$ are A_2'', E″, E″, A_1'', E″, E″ (occupied orbitals) and E″, E″, A_2'', E″, E″, A_1'' (empty orbitals).

2.1% (ν_4, 705 cm^{-1}), while the only e_{1g} vibration (ν_{10}, 859 cm^{-1}) is responsible for 0.6% of the observed activity. We can compare the experimental intensities with our predictions for benzene, resulting from CNDO/S + CIS 15 × 15 calculations: 74.1% (ν_8), 9.4% (ν_9), 12.9% (ν_6), and 2.3% (ν_7) for e_{2g} modes, 0.2% (ν_5), and 0.9% (ν_4) for b_{2g} modes, and 0.1% for the e_{1g} vibration ν_{10}. Although not as accurate as ab initio multiconfiguration quadratic response-theory calculations,[19] our CNDO/S + CIS results are satisfactory: the dominant activity of the ν_8 vibration is well reproduced, as well as the remaining e_{2g} activity. We notice an intensity underestimate for the ν_9 vibration and an intensity overestimate for the ν_6 *CCC* bending vibration. Finally, concerning out-of-plane modes, the trend shown by CNDO/S + CIS results points to a general underestimate of vibronically induced intensities. With the above considerations in mind, we are ready to analyze the phosphorescence spectra of TN and TPH. The T_1 and S_0 states of TN belong to A′ symmetry, the transition dipole moment operator belongs to E′ and A″ symmetries, while the SO operator transforms like A′ and E″ symmetry representations. Hence, the HT-active vibrations of TN belong to (E′,A″ × A′,E″) = e′,a″,e″ symmetries. Vibronically induced oscillator strengths were computed, along the lines outlined in section 3 (CNDO/S + CIS 42 × 41 calculations), for every NTS mode of appropriate symmetry. The results are collected in Table 4. In the same table, the FC activity of TS modes is represented by the γ_i values computed on the basis of QCFF/PI optimized structures. These computed HT and FC activities were employed to model the phosphorescence spectrum of TN: two simulations (spectra B and C) are depicted in the bottom part of Figure 2. Spectrum B was plotted with a Lorenzian line width of 40 cm^{-1} to simulate the line broadening observed at 77 K. To get a better view of the structure hidden under the broad bands, the phosphorescence spectrum was also plotted with a line width of 3 cm^{-1} (spectrum C in Figure 2). Inspection of the figure shows that the similarity between spectrum A (observed) and spectrum B (computed) is rather impressive: only one strong band dominates the two spectra accompanied by a rich, but comparably weaker, vibronic structure. Interestingly, the simulation also accounts for the shoulder on the blue side of the strong band observed at 474.9 nm. The high-resolution simulated spectrum in Figure 2 shows that the strong observed band is due to the computed 1629 cm^{-1} vibration. The molecular motion responsible for the activity of the latter is shown in Figure 4: it corresponds to a moderately perturbed ν_8 vibration of benzene localized on the central benzenic ring of TN. Similarly, the shoulder on the blue side of the 474.9 nm band is due to *CC* stretchings which correspond to combinations of the ν_8 mode localized on the remaining three benzenic rings. Inspection of the high-resolution simulation in Figure 2 shows, indeed, a fine structure formed by three bands due to the 1600, 1489, and 1410 cm^{-1} computed frequencies.

Of some interest is the low-wavelength region of the spectrum, where additional false origins are observed. Six weak bands are observed and, although slightly more structured, six bands are also predicted by the simulations. A cursory

TABLE 4: Computed and Observed Ground-State Vibrational Frequencies (cm^{-1}, *CH* Stretchings Not Included) of Truxene and Associated Franck−Condon and Herzberg−Teller Activity in the $T_1 \rightarrow S_0$ Transition

a′			e′			a″			e″	
ν_{calc}[a]	γ[b]	ν_{obs}[c]	ν_{calc}[a]	$f^d \times 10^{10}$	ν_{obs}[c]	ν_{calc}[a]	$f^d \times 10^{10}$	ν_{obs}[c]	ν_{calc}[a]	$f^d \times 10^{10}$
1605	0.11	1610	1629	1.308	1608	1169	0.004		1168	0.004
1567	0.04		1600	0.188		1059	0.005		1059	0.017
1491	0.05		1566	0.000	1578	1019	0.001	1008	1019	0.003
1485		1475	1489	0.055		982	0.002	942	981	0.004
1472		1475	1483	0.007	1473	911	0.013	916	910	0.016
1404	0.03	1395	1474	0.009	1459	785	0.010	782	784	0.022
1336	0.03		1410	0.055	1391	727	0.090	736	690	0.008
1294	0.03	1307	1306	0.003	1317	649	0.002		592	0.028
1279		1248	1287	0.020		496	0.016		484	0.008
1247		1223	1222	0.010	1221	421	0.005	419	420	0.009
1194	0.05	1191	1181	0.031	1199	277	0.027		355	0.000
1156			1156	0.015	1162	230	0.073		252	0.005
1148			1150	0.014		105	0.014		136	0.005
1086			1089	0.010	1098	47	0.031		65	0.127
1040		1034	1037	0.007	1026					
1031	0.01	1009	988	0.110	994					
839	0.01	834	825	0.001	856					
769			796	0.031						
677	0.04		620	0.063	627					
670	0.10		575	0.030	584					
542			516	0.022						
345			305	0.093						
254	0.03		118	0.001						

[a] From QCFF/PI[9] calculations. [b] FC activity in the $T_1 \rightarrow S_0$ transition, from QCFF/PI calculations. [c] Observed IR and Raman bands, from ref 17. [d] HT induced activity in the $T_1 \rightarrow S_0$ transition, from CNDO/S + CIS 42 × 41 calculations

TABLE 5: Computed and Observed Ground-State Vibrational Frequencies (cm^{-1}, *CH* Stretchings Not Included) of Triphenylene and Associated Franck−Condon and Herzberg−Teller Activity in the $T_1 \rightarrow S_0$ Transition

a_1'				a_2'				e′			
ν_{calc}[a]	γ[b]	ν_{obs}[c]	ν_{obs}[d]	ν_{calc}[a]	$f^e \times 10^{10}$	ν_{obs}[c]	ν_{obs}[d]	ν_{calc}[a]	$f^e \times 10^{10}$	ν_{obs}[c]	ν_{obs}[d]
1541		1550		1582		1560		1591	2.323	1611	1612
1464	0.03	1458	1471	1472		1422	1423	1559	0.540	1579	1588
1292	0.20	1341	1347	1346		1320	1315	1509	0.009	1500	1502
1216	0.03	1230		1127		1136		1456	0.002	1434	1435
1180		1180		984		1025	1022	1347	0.097	1300	1301
1079	0.02	1062		625		607		1276	0.086	1255	1256
718	0.05	700		549		550		1252	0.100	1245	1247
431	0.01	418						1168	0.038	1167	1173
								1103	0.018	1110	1106
								1062	0.013	1052	1022
								1019	0.094	1003	1005
								774	0.084	776	
								630	0.045	619	622
								392	0.241	410	406
								259	0.034	264	264

a_1''				a_2''				e″			
ν_{calc}[a]	$f^e \times 10^{10}$	ν_{obs}[c]	ν_{obs}[d]	ν_{calc}[a]	$f^e \times 10^{10}$	ν_{obs}[c]	ν_{obs}[d]	ν_{calc}[a]	$f^e \times 10^{10}$	ν_{obs}[c]	ν_{obs}[d]
1050	0.001	951	966	1001	0.000	946		1052	0.002	972	993
884	0.003	868	868	764	0.000	740		999	0.000	936	
747	0.000	711		417	0.012	427	421	880	0.001	850	
532	0.016	570	569	126	0.006	152		779	0.000	758	
134	0.053	135	145					676	0.012		642
								521	0.032	532	542
								436	0.002	431	
								279	0.029	282	
								79	0.090		121

[a] From QCFF/PI[9] calculations. [b] FC activity in the $T_1 \rightarrow S^0$ transition, from QCFF/PI calculations. [c] IR and Raman observed bands from crystalline triphenylene, from ref 3. [d] Bands observed in the phosphorescence spectrum of ref 2. [e] HT induced activity in the $T_1 \rightarrow S_0$ transition, from CNDO/S + CIS 42 × 42 calculations.

examination of the induced oscillator strengths listed in Table 4 shows that most of the activity is due to in-plane e′ vibrations. Nevertheless, on the basis of computed results, some intensity from low-frequency out-of-plane vibrations is suggested to contribute to the first, second, and fourth broad bands of the observed spectrum. A summary of the proposed assignments is reported in Table 1. The vibronic structure in the higher wavelength region of the phosphorescence spectrum, above 474.9 nm, can only be due to combination bands since *CH* stretching activity is negligible. In this region, TS vibrations are expected to contribute and we assign the observed bands on the basis of computed FC activities (γ values). Even in this

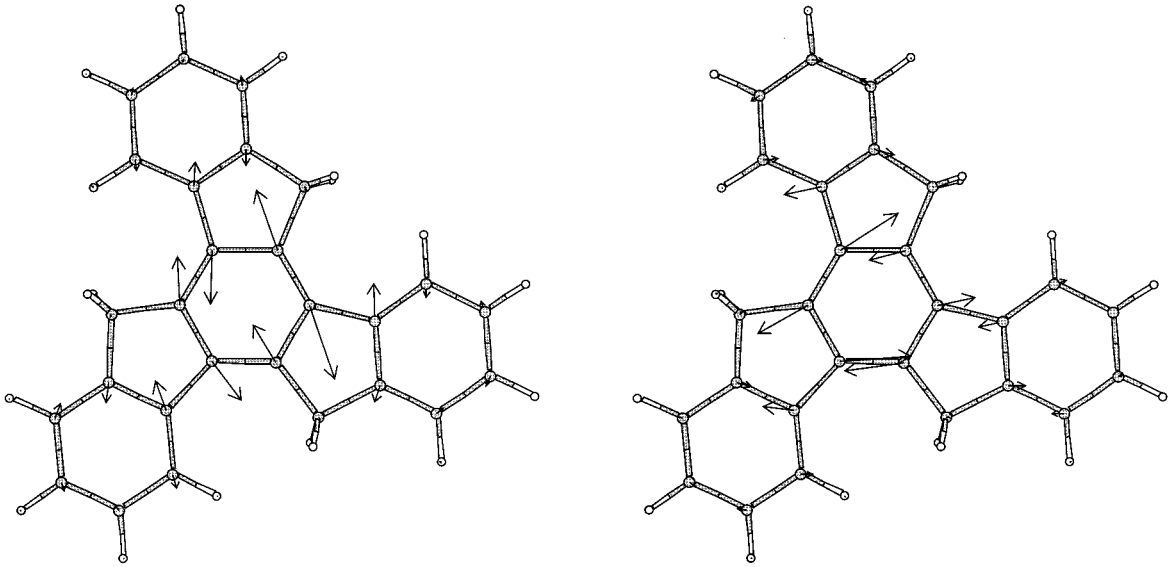

Figure 4. Molecular motion associated with the 1629 cm^{-1} computed e′ vibrational frequency of truxene: (a) first and (b) second component of the doubly degenerate mode.

region the accuracy of the simulation is remarkable: the largest computed γ parameter is 0.11 and, indeed, the strongest intensity observed above 475 nm is ca. $^1/_{10}$ of the 474.9 nm band. As summarized in Table 1, all the observed bands in this spectral region can be assigned in terms of combinations of the 1588 cm^{-1} e′ fundamental with a′ frequencies. The only major intensity deviation with respect to the observed spectrum occurs for the last (highest wavelength) computed band, whose intensity is overestimated by the calculations. Similarly to TN, the phosphorescence spectrum of TPH also shows an isolated strong band surrounded by a weaker vibronic structure. The T_1 and S_0 states of TPH belong to A_2' and A_1' symmetries, respectively, the transition dipole moment operator belongs to E′ and A_2'' symmetries, while the SO operator transforms like A_2' and E″ symmetry representations. Hence, the HT-active vibrations in the phosphorescence spectrum of TPH belong to

$$[\Gamma_\mu(E',A_2'') \times \Gamma_{SO}(A_2',E'') \times \Gamma_{T_1}(A_2')] = e',a_2'',a_1'',e''$$

symmetries. TPH being slightly smaller than TN, we could carry out full valence CIS calculations (42 × 42). The computed HT and FC activities employed to model the phosphorescence spectrum of TPH are collected in Table 5. The correspondingly simulated low-resolution (line width of 50 cm^{-1}) and high-resolution (line width of 3 cm^{-1}) spectra are presented in the bottom part of Figure 3, spectra B and C, respectively. A comparison between the observed high-resolution phosphorescence spectrum of ref 2 and the simulated vibronic structure (line width 3 cm^{-1}) is shown in Figure 5.

A cursory comparison between observed and simulated spectra in Figure 3 shows that, similarly to TN, the simulation accounts remarkably well for the strong band observed at 462.1 nm. The high-resolution spectrum reveals that two vibrational modes of e′ symmetry, whose computed frequencies are 1559 and 1591 cm^{-1}, contribute to the strong band. These two vibrations correspond to the 1588 and 1602 cm^{-1} fundamentals observed in the high-resolution spectrum of ref 2. Interestingly, in agreement with the intensities observed in ref 2, the calculations predict the first mode to be considerably less active than the second. A pictorial view of the molecular motion associated with the strongly active normal mode (1591 cm^{-1}) is presented in Figure 6. As expected, the mode bears a

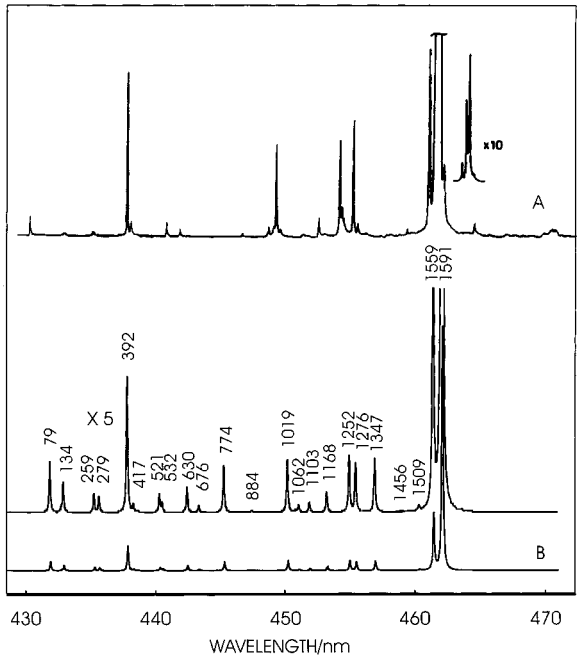

Figure 5. High-resolution phosphorescence spectrum of triphenylene: (A) experimental spectrum from ref 2; (B) simulated spectrum (line width 3 cm^{-1}, 0−0 transition at 23231 cm^{-1}).

parentage with the ν_8 of benzene, but in contrast with TN, the TPH motion is almost uniformly delocalized over the four fused benzene rings.

The remaining three combinations of the ν_8 mode are also active in the spectrum, although with only moderate intensity: these *CC* stretchings correspond to the computed 1559, 1347, and 1252 cm^{-1} vibrational frequencies. As discussed above, the first (1559 cm^{-1}) contributes to the intensity of the main band in the spectrum of Figure 3. Conversely, the last two vibrations contribute to the band observed at 454.9 nm. According to calculations, an additional mode contributes significantly to the 454.9 nm band: the computed 1276 cm^{-1} vibration. Inspection of the high-resolution spectrum of ref 2 (spectrum A in Figure 5) shows, indeed, three bands at 1247, 1256, and 1301 cm^{-1} which are readily assigned to the 1252, 1276, and 1347 cm^{-1} computed e′ vibrations. This attribution

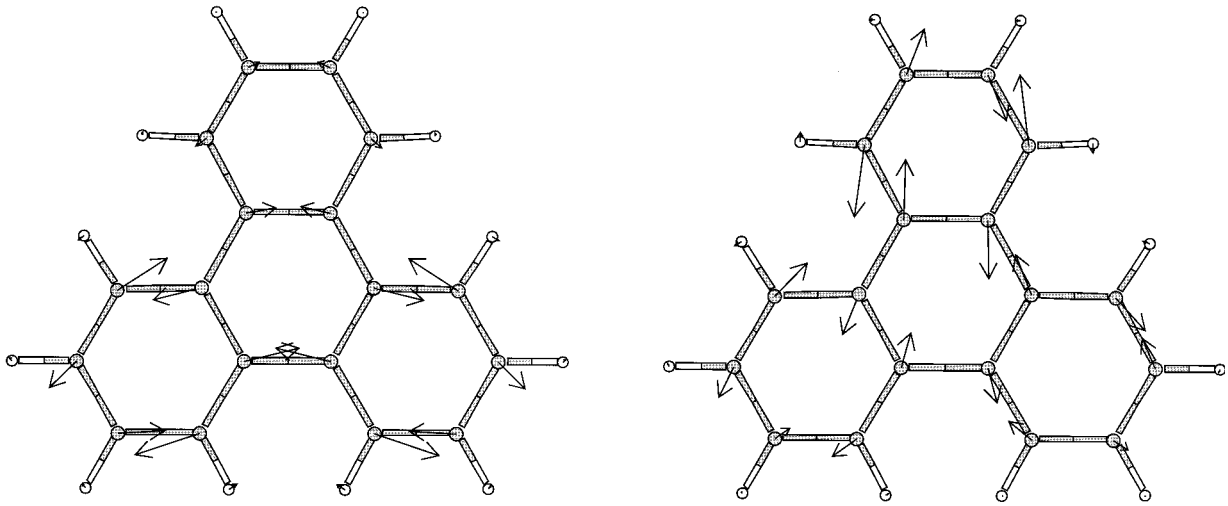

Figure 6. Molecular motion associated with the 1591 cm^{-1} computed e′ vibrational frequency of triphenylene: (a) first and (b) second component of the doubly degenerate mode.

supports the reassignment already discussed in section 4 of the observed 1256 cm^{-1} fundamental to e′ symmetry. The force-field calculations show that this mode is dominated by the ν_{14} of benzene, which explains the weaker observed intensity[2] compared to the remaining e′ vibrations in the same frequency region. A comparison with the correspondingly computed intensity shows an overestimate which is probably the result of unbalanced QCFF/PI mixing between the modes associated with the two very close computed frequencies (1252 and 1276 cm^{-1}). Besides the 454.9 nm band, in the low-wavelength region three additional bands are observed. The bands at 437.4 and 449.2 nm are assigned to the computed 392 and 1019 e′ active vibrations, respectively. According to calculations, the first broad band in the spectrum (431.0 nm) receives a contribution from out-of-plane vibrations which probably overlaps with the weak 0−0 band. The latter may become weakly active, in TPH as well as TN, as a result of symmetry lowering induced by matrix perturbations. The vibronic activity in this region of the spectrum is well reproduced by the simulations, although we notice a general intensity underestimate. The computed HT activity (Figure 5) also compares remarkably well with the vibronic structure observed in the high-resolution phosphorescence spectrum of ref 2. This enables us to assign the weak bands observed in ref 2 at 542, 642, and 993 cm^{-1} to e″ fundamentals and the 145 cm^{-1} band to the lowest a_1″ fundamental (see Table 5). The major deviation between simulated and observed spectra concerns the intensity computed at 774 cm^{-1}, a region where little activity is observed. Inspection of the molecular motion associated with the computed 774 cm^{-1} e′ fundamental reveals that this mode corresponds to a combination of ν_6 of benzene delocalized over the benzenic rings of TPH. Hence, the overestimate of its activity is likely to be connected with the computed overestimate of the ν_6 activity in benzene discussed at the beginning of this section. An interesting aspect of the phosphorescence spectrum shown in Figure 3 is that it extends to the spectral region were combination bands contribute intensity. We have simulated the activity in this region (above 463 nm) by employing the computed FC activities listed in Table 5. The comparison between observed and simulated spectra (Figure 3, spectra A and B) is also very satisfactory in this region. As summarized in Table 1, the first three weak bands in the spectrum at 470.7, 478.0, and 485.4 nm are assigned to the first member of progressions of TS modes (431, 718, and 1079 cm^{-1} computed frequencies) built on the 1591 cm^{-1} (computed) e′ false origin. The last band observed in the spectrum at 492.5 nm is sensibly more intense than the previous three, a feature which is nicely reproduced by the simulation.

From the above discussion we can conclude that the combination of experimental and computational investigation has led to a clear understanding of the vibronic activity in the phosphorescence spectra of the two disklike aromatic molecules. A detailed analysis of the individual terms that contribute to the sums in equation 2 is beyond the scope of this work. However, according to equation 2, the $T_1 \rightarrow S_0$ transition dipole moment results from two contributions: $M_{S_0,T_1} = S + T$, the first of which (*S*) *steals* intensity from singlet−singlet transitions while the second (*T*) *steals* intensity from triplet−triplet transitions. It is of some interest to examine which of the two contributes most to the activity induced in the phosphorescence spectra of the aromatic molecules considered here. To this end we have analyzed the most active vibrations of benzene (e_{2g}), TPH (e′), and TN (e′) and listed separately the two contributions *S* and *T* in Table 6. The vibronically induced activities are out-of-plane polarized (*z*) and nonzero for the triplet sublevels *x* and *y*. Thus, in Table 6, we list only the $(\partial M_z^{x,y}/\partial Q)$ contributions, corresponding to one of the two components of the doubly degenerate mode.

A survey of the data in Table 6 shows that for TPH and benzene, the *T* contribution is on average at least 3 times larger than the *S* contribution. This implies that most of the intensity observed for in-plane modes of *e* symmetry is stolen from triplet−triplet allowed transitions. The situation is less straightforward in the case of TN, for which similar *S* and *T* contributions are calculated. This might suggest that slightly different mechanisms are operative in bringing intensity to the phosphorescence of TN compared to TPH and benzene. However, this result should be taken with caution since the CIS calculations performed for TN did not include the full valence orbital space. To explore the effect of CIS size increase, we evaluated the *S* and *T* contributions for the 1629 cm^{-1} mode of TN with a larger orbital space (48 × 48) and obtained: $(\partial M_z^x/\partial Q)$ $(S) = -0.496 \times 10^{-4}$; $(\partial M_z^x/\partial Q)$ $(T) = -1.220 \times 10^{-4}$; $(\partial M_z^y/\partial Q)$ $(S) = -0.226 \times 10^{-4}$; $(\partial M_z^y/\partial Q)$ $(T) = -0.235 \times 10^{-4}$ e/amu$^{1/2}$. These values suggest that the dominant contribution of the *T* term computed for benzene and TPH is also recovered for TN by increasing the size of CIS calculations toward the full valence orbital space limit.

TABLE 6: Computed *S* and *T* Contributions to the Vibronically Induced $T_1 \rightarrow S_0$ Transition Moment of Triphenylene, Truxene, and Benzene (In-Plane Active Modes Only)

triphenylene (e′)

ν^a	$(\partial M_z^x/\partial Q)^{b,c}$	$(\partial M_z^y/\partial Q)^{b,c}$	ν^a	$(\partial M_z^x/\partial Q)^{b,c}$	$(\partial M_z^y/\partial Q)^{b,c}$
1591	−0.004 (*S*)	−0.578 (*S*)	1103	−0.010 (*S*)	−0.034 (*S*)
	−0.008 (*T*)	−1.636 (*T*)		−0.038 (*T*)	−0.122 (*T*)
1559	0.028 (*S*)	0.264 (*S*)	1062	−0.028 (*S*)	−0.002 (*S*)
	0.828 (*T*)	0.774 (*T*)		−0.108 (*T*)	−0.004 (*T*)
1509	−0.006 (*S*)	0.038 (*S*)	1019	−0.012 (*S*)	−0.082 (*S*)
	−0.016 (*T*)	0.092 (*T*)		−0.040 (*T*)	−0.268 (*T*)
1456	−0.020 (*S*)	−0.002 (*S*)	774	−0.012 (*S*)	−0.068 (*S*)
	0.042 (*T*)	−0.006 (*T*)		−0.036 (*T*)	−0.220 (*T*)
1347	0.060 (*S*)	−0.060 (*S*)	630	0.006 (*S*)	0.038 (*S*)
	0.222 (*T*)	−0.216 (*T*)		0.022 (*T*)	0.148 (*T*)
1276	0.010 (*S*)	0.104 (*S*)	392	0.064 (*S*)	−0.038 (*S*)
	0.026 (*T*)	0.268 (*T*)		0.234 (*T*)	−0.138 (*T*)
1252	0.082 (*S*)	−0.030 (*S*)	259	0.014 (*S*)	−0.014 (*S*)
	0.292 (*T*)	−0.106 (*T*)		0.060 (*T*)	−0.056 (*T*)
1168	0.044 (*S*)	0.002 (*S*)			
	0.194 (*T*)	0.002 (*T*)			

truxene (e′)

ν^a	$(\partial M_z^x/\partial Q)^{b,d}$	$(\partial M_z^y/\partial Q)^{b,d}$	ν^a	$(\partial M_z^x/\partial Q)^{b,d}$	$(\partial M_z^y/\partial Q)^{b,d}$
1629	−0.774 (*S*)	−0.278 (*S*)	1150	0.024 (*S*)	−0.054 (*S*)
	−0.968 (*T*)	−0.258 (*T*)		0.028 (*T*)	−0.084 (*T*)
1600	0.140 (*S*)	−0.230 (*S*)	1089	0.054 (*S*)	−0.008 (*S*)
	0.162 (*T*)	−0.302 (*T*)		0.070 (*T*)	−0.006 (*T*)
1566	0.006 (*S*)	0.020 (*S*)	1037	−0.042 (*S*)	−0.030 (*S*)
	−0.020 (*T*)	−0.044 (*T*)		−0.050 (*T*)	−0.014 (*T*)
1489	−0.092 (*S*)	−0.110 (*S*)	988	−0.096 (*S*)	−0.164 (*S*)
	−0.138 (*T*)	−0.124 (*T*)		−0.128 (*T*)	−0.154 (*T*)
1483	0.026 (*S*)	−0.042 (*S*)	825	−0.010 (*S*)	0.004 (*S*)
	0.014 (*T*)	−0.068 (*T*)		−0.020 (*T*)	0.002 (*T*)
1474	−0.018 (*S*)	0.074 (*S*)	796	0.066 (*S*)	−0.014 (*S*)
	−0.012 (*T*)	0.056 (*T*)		0.116 (*T*)	−0.028 (*T*)
1410	0.062 (*S*)	0.134 (*S*)	620	0.098 (*S*)	−0.028 (*S*)
	0.082 (*T*)	0.164 (*T*)		0.122 (*T*)	−0.060 (*T*)
1306	−0.044 (*S*)	0.000 (*S*)	575	0.058 (*S*)	0.016 (*S*)
	−0.030 (*T*)	−0.020 (*T*)		0.096 (*T*)	0.014 (*T*)
1287	−0.022 (*S*)	−0.084 (*S*)	516	0.048 (*S*)	0.014 (*S*)
	−0.032 (*T*)	−0.094 (*T*)		0.074 (*T*)	0.014 (*T*)
1222	−0.042 (*S*)	0.054 (*S*)	305	0.078 (*S*)	0.004 (*S*)
	−0.016 (*T*)	0.064 (*T*)		0.122 (*T*)	0.000 (*T*)
1181	−0.090 (*S*)	0.056 (*S*)	118	0.002 (*S*)	0.004 (*S*)
	−0.088 (*T*)	0.086 (*T*)		0.004 (*T*)	0.006 (*T*)
1156	−0.022 (*S*)	0.064 (*S*)			
	−0.034 (*T*)	0.074 (*T*)			

benzene (e_2)

ν^a	$(\partial M_z^x/\partial Q)^{b,e}$	$(\partial M_z^y/\partial Q)^{b,e}$	ν^a	$(\partial M_z^x/\partial Q)^{b,e}$	$(\partial M_z^y/\partial Q)^{b,e}$
3090	0.000 (*S*)	−0.024 (*S*)	1145	−0.162 (*S*)	−0.002 (*S*)
	0.000 (*T*)	0.632 (*T*)		−0.590 (*T*)	−0.002 (*T*)
1572	−0.692 (*S*)	0.000 (*S*)	610	0.156 (*S*)	0.000 (*S*)
	−1.830 (*T*)	0.008 (*T*)		0.518 (*T*)	−0.006 (*T*)

[a] From QCFF/PI[9] calculations. [b] $\times 10^4$ e/amu$^{1/2}$. [c] HT induced activity in the $T_1 \rightarrow S_0$ transition, from CNDO/S + CIS 42 × 42 calculations. [d] HT induced activity in the $T_1 \rightarrow S_0$ transition, from CNDO/S + CIS 42 × 41 calculations. [e] HT induced activity in the $T_1 \rightarrow S_0$ transition, from CNDO/S + CIS 15 × 15 calculations.

Besides the unusual structure of their phosphorescence spectra, the lowest triplet states of TPH and TN are also interesting for their lifetimes which are among the longest known: 14 s was measured for TPH in MCH at 77 K,[7] and 13.3 s was obtained for TN in ethanol.[17] Radiative triplet lifetimes can be extracted from total lifetimes if the $S_1 \rightarrow T_1$ intersystem crossing (ISC) and phosphorescence quantum yields are available. For triphenylene, $\phi_P = 0.5$ at 77 K and $\phi_{ISC} = 0.95$.[13] Thus, $\tau_P^0 = (\phi_{ISC}\ \tau_P)/\phi_P = 27$ s, very close to the commonly accepted value for benzene (ca. 30 s[20]). The radiative phosphorescence lifetimes of TN and TPH can be readily evaluated from computed oscillator strengths with eq 7. The T_1 radiative lifetime of TN in ethanol ($n = 1.36$[21]) is computed to be 21 s, while that of TPH in MCH ($n = 1.42$[21]) is 12 s. The values are in good agreement with the experimental data of 13.3 and 14 s. However, if we take into account the contribution of nonradiative processes to the latter data, we can conclude that the computed values are slightly underestimated, a result which seems to be typical of the method: the radiative triplet lifetime of benzene is computed to be 12 s (observed ca. 30 s[20]), and the radiative triplet lifetime of C_{70} is computed to be 9 s (observed 40 s).[8]

6. Conclusions

The phosphorescence spectra of triphenylene and truxene, recorded in glassy solvents, show a similar structure, dominated by a strong band at about 1600 cm^{-1} surrounded by a rich but comparably weaker vibronic structure. The vibronic activity in the spectra was successfully simulated with the help of semiempirical quantum-chemical calculations which included the effect of spin−orbit along with vibronic perturbations. The molecular motions responsible for the strongest activity in the spectra were identified: they correspond to the ν_8 vibration of benzene delocalized over the four benzenic rings in the case of TPH and localized over the central benzenic ring in the case of TN. Besides the strong band in the spectra, the simulations also account very well for the weaker observed intensities and contribute to improve the identification of the ground-state frequencies of the two disklike molecules. Although more sophisticated (ab initio) calculations will be required to more firmly establish the symmetry of the equilibrium structures of TN and TPH in T_1, the present analysis of their phosphorescence spectra strongly suggests that the two systems, similarly to benzene, are not permanently distorted in one lower-symmetry conformation. The analysis of the activities computed for HT-active in-plane modes reveals that $^3/_4$ of the induced intensity is derived from triplet−triplet transition dipole moments while only the remaining $^1/_4$ is stolen from singlet−singlet transitions. The calculations indicate a similar trend for TPH, TN, and benzene. The encouraging results obtained here suggest that our theoretical approach might be successfully applied to analyze the effect of substituents on the photophysical properties of derivatives of TPH and TN, which are of greater interest in the field of material science.

Acknowledgment. This work was partially supported by a grant from the Danish National Science Research Council to the Center for Molecular Dynamics and Laser Chemistry. F.N. and G.O. gratefully acknowledge financial support from the University of Bologna (Funds for selected research topics: Project "Materiali innovativi") and from CNR (Project "Applicazioni di spettroscopie ottiche").

References and Notes

(1) Markovitsi, D.; Germain, A.; Millie, P.; Lecuyer, P.; Gallos, L. K.; Argyrakis, P.; Bengs, H.; Ringsdorf, H. *J. Phys. Chem.* **1995**, *99*, 1005. Marguet, S.; Markovitsi, D.; Millie, P.; Sigal, H. *J. Phys. Chem. B* **1998**, *102*, 4697.

(2) Nishi, N.; Matsui, K.; Kinoshita, M.; Higuchi, J. *Mol. Phys.* **1979**, *38*, 1.

(3) Schettino, V. *J. Mol. Spectrosc.* **1970**, *34*, 78.

(4) Krumschmidt, H.; Kryschi, C. *Chem. Phys.* **1991**, *154*, 459.

(5) Zgierski, M. Z. *Chem. Phys. Lett.* **1980**, *69*, 608.

(6) Lang, K. F.; Zander, M.; Theiling, E. A. *Ber.* **1960**, *93*, 321.

(7) Baunsgaard, D.; Larsen, M.; Harrit, N.; Frederiksen, J.; Wilbrandt, R.; Stapelfeldt, H. *J. Chem. Soc., Faraday Trans.* **1997**, *93*, 1893.

(8) Negri, F.; Orlandi, G. *J. Phys. B: At. Mol. Opt. Phys.* **1996**, *29*, 5077.

(9) Negri, F.; Orlandi, G. *J. Phys. B: At. Mol. Opt. Phys.* **1996**, *29*, 5049.

(10) Warshel, A.; Karplus, M. *J. Am. Chem. Soc.* **1972**, *94*, 5612.

(11) Del Bene, J.; Jaffé, H. H. *J. Chem. Phys.* **1968**, *48*, 1807.

(12) Masmanidis, C. A.; Jaffé, H. H.; Ellis, R. L. *J. Phys. Chem.* **1975**, *79*, 19.

(13) Gilbert, A.; Baggot, J. *Essentials of molecular photochemistry*; Blackwell Scientific Publications: Bostom, MA, 1991.

(14) Buma, W. J.; van der Waals, J. H.; van Hemert, M. C. *J. Chem. Phys.* **1990**, *93*, 3733.

(15) The stabilization of benzene is computed to be 100 cm^{-1} by QCFF/PI, compared to the more accurate value of 800 cm^{-1} from ref 14.

(16) Chojnacki, H.; Laskowski, Z.; Lewanowicz, A.; Ruziewicz, Z.; Wandas, R. *Chem. Phys. Lett.* **1986**, *124*, 478.

(17) Frederiksen, J. Ph.D. Thesis, Risø National Laboratory and Department of Chemistry, University of Copenhagen, 1996.

(18) Albrecht, A. C. *J. Chem. Phys.* **1963**, *38*, 354. Nieman, G. C. *J. Chem. Phys.* **1969**, *50*, 1660.

(19) Minaev, B. F.; Knuts, S.; Ågren, H.; Vahtras, O. *Chem. Phys.* **1993**, *175*, 245. Knuts, S.; Minaev, B. F.; Ågren, H.; Vahtras, O. *Theor. Chim. Acta* **1994**, *87*, 343.

(20) Lim, E. C. *J. Chem. Phys.* **1962**, *36*, 3497.

(21) *CRC Handbook of Chemistry and Physics*, 1972.